



High strain rate effects on direct tensile behavior of high performance fiber reinforced cementitious composites



Tuan Kiet Tran, Dong Joo Kim *

Sejong University, Department of Civil and Environmental Engineering, 143-747 Seoul, Republic of Korea

ARTICLE INFO

Article history:

Received 24 January 2013

Received in revised form 2 August 2013

Accepted 4 October 2013

Available online 12 October 2013

Keywords:

Strain energy impact test system

High strain rates

High performance fiber reinforced

cementitious composites

Dynamic increase factor

Strain rate effect

ABSTRACT

Direct tensile behavior of high performance fiber reinforced cementitious composites (HPFRCCs) at high strain rates between 10 s^{-1} and 30 s^{-1} was investigated using strain energy frame impact machine (SEFIM) built by authors. Six series of HPFRCC combining three variables including two types of fiber, hooked (H) and twisted (T) steel fiber, two fiber volume contents, 1% and 1.5%, and two matrix strengths, 56 MPa and 81 MPa, were investigated. The influence of these three variables on the high strain rate effects on the direct tensile behavior of HPFRCCs was analyzed based on the test results. All series of HPFRCCs showed strongly sensitive tensile behavior at high strain rates, i.e., much higher post cracking strength, strain capacity, and energy absorption capacity at high strain rates than at static rate. However, the enhancement was different according to the types of fiber, fiber volume content and matrix strength: HPFRCCs with T-fibers produced higher impact resistance than those with H-fibers; and matrix strength was more influential, than fiber contents, for the high strain rate sensitivity. In addition, an attempt to predict the dynamic increase factor (DIF) of post cracking strength for HPFRCCs considering the influences of fiber type and matrix strength was made.

© 2013 Elsevier Ltd. All rights reserved.

1. Introduction

High performance fiber reinforced cement composites (HPFRCCs) are characterized with high tensile resistance and energy absorption capacity due to their unique strain hardening behavior [1]. Based on the high tensile resistance and energy absorption capacity of HPFRCCs, in comparison with concrete or normal fiber reinforced concrete (FRC), the resistance of civil infrastructure under high rate loads is expected to be enhanced by applying HPFRCCs. However, the mechanical response of these structures using HPFRCCs under high rate loads such as impact or blast is not predictable using the mechanical properties tested at static strain rate [2]. Thus, the mechanical response of HPFRCCs in wide range of strain rates should be clearly understood to enhance the resistance of civil infrastructure at high rate loads.

The impact and blast resistance of civil infrastructure is important when considering the possibility of extreme events, including those due to terrorism. Understanding the behavior of HPFRCCs at the high strain rates and dynamic loading will be helpful in the enhancement of the resistance of civil infrastructure under extreme loadings, including projectile impact and blast, for HPFRCCs to be applied in potentially vulnerable structures, such as

skyscrapers, nuclear reactor containment vessels, and offshore platforms.

Although much research has been performed on the direct tensile behavior for cement-based material, the investigated strain rates were mostly lower than seismic strain rates [3–7]. Fig. 1 presents a schematic diagram of the range of strain rates including the meaning of seismic strain rates that are typically of interest to material scientists [8]. There are very few studies concerning with the direct tensile behavior at high strain rates, especially for HPFRCCs using high strength deformed steel fibers. Recently, Cadoni et al. [9] studied tensile behavior of FRC reinforced with two different types of fiber, PVA and steel, at high strain rates from 50 s^{-1} to 200 s^{-1} using a modified Hopkinson bar (MHB). They reported that the tensile strength of FRC with steel fibers was significantly enhanced with increasing strain rate while that of FRC with PVA fibers showed less rate sensitivity. Caverzan et al. [10] also used the MHB to investigate the tensile behavior FRC with high carbon straight steel fiber at high strain rates up to 300 s^{-1} .

Mechtcherine et al. [11] investigated, by using high rate MTS hydraulic testing machine, the tensile behavior of strain-hardening cement-based composites (SHCC) reinforced by PVA fibers at rates ranging up to 50 s^{-1} . SHCC with PVA fibers showed a considerable increase in both tensile strength and strain capacity at high strain rates. Zhu et al. [12], also using the hydraulic testing machine, investigated the Young's modulus, tensile strength, maximum strain, and toughness of the AR-glass fabric–cement composite at wide strain rate between 2.2×10^{-5} and 24 s^{-1} .

* Corresponding author. Tel.: +82 2 3408 3820.

E-mail address: djkim75@sejong.ac.kr (D.J. Kim).

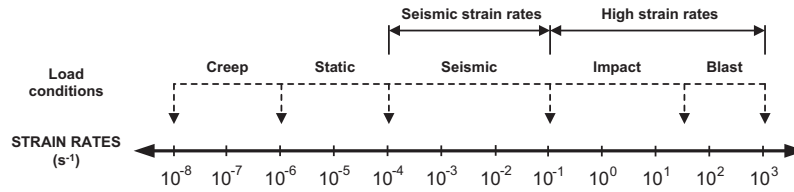


Fig. 1. Strain rate regimes.

The main reason for the lack of studies on the direct tensile behavior of material at high rate loading is the complete absence of a standardized tensile test set-up at high strain rates [2]. In addition, the relatively large size specimen for HPFRCCs can be the other reason because HPFRCCs require large size specimens enough to represent reasonably the behavior of composite materials containing fibers. However, the large-size specimen produces a considerable inertia effect due to gravity, if the test set-up was vertically installed, on the estimation of pure material response. Even though both MHB and high rate hydraulic machine may resolve the problem, they still require very high cost and large space to be installed.

To resolve the limitations of current impact test systems above mentioned, including restriction of inertia effect and reduction of cost, a new impact test set-up named strain energy frame impact machine (SEFIM), which has ability of testing large size specimens with a relatively small device, was built by authors [13], as shown in Fig. 2. Unlike current impact test techniques, SEFIM utilizes a strain energy storage frame to generate high rate impact pulse. The use of energy frame instead of bar not only reduces the size of system leading to the reduction of cost and installation space, but also delivers a higher rate tensile stress wave. Moreover, the machine was designed in horizontal direction, thereby can remove the gravity effect due to the large-size specimen as mentioned above. In particular, since the transmitter bar is connected directly to specimen, the stress wave from specimen will propagate directly to transmitter bar without any distortion. Thus, the signal that obtaining from the strain gauges attached on transmitter bar, in this case, reflects pure material resistance. Finally, this machine can test the specimen with the size and boundary condition as same as static test.

By using this machine, Tran and Kim [14] recently reported how to obtain the direct tensile stress versus strain response of HPFRCCs at high strain rates between 10 s^{-1} and 40 s^{-1} . They also discussed that the interfacial bond strength between fiber and matrix was a key factor for the rate sensitive behavior of HPFRCCs.

However, the previous research performed by authors did not focus on the influencing parameters for rate sensitive tensile behavior of HPFRCCs. The role of fiber type, fiber volume content and matrix strength on the rate sensitive behavior of HPFRCCs is not clearly understood yet. This research is initiated toward a

deeper understanding of the strain rate effects on direct tensile behavior of HPFRCCs using high strength deformed steel fibers, with a focus on the effect of matrix, fiber type and volume content. Specific objectives are to (1) investigate the high strain rate effects on tensile behavior of HPFRCCs using SEFIM, (2) evaluate the effect of fiber type, fiber volume content and matrix strength on the rate sensitivity of HPFRCCs, and (3) propose an equation to predict the DIF of post cracking strength of HPFRCCs.

2. Experimental program

An experimental program including six series of tensile specimen was designed to investigate the role of matrix, fiber type and fiber volume content in the rate sensitive behavior of HPFRCCs using deformed steel fibers as shown in Table 3. A flowchart summarizing this experimental program and test series is described in Fig. 3. A universal test machine was applied for the static test at the strain rate of $\dot{\epsilon} = 0.000167 \text{ s}^{-1}$ for tensile specimens with 100 mm gauge length while SEFIM was used for the impact tests at higher strain rates between 10 s^{-1} and 30 s^{-1} . The detail procedure for obtaining tensile stress versus strain response at the higher strain rates was recently reported by authors [12,13].

2.1. Material and specimen preparation

Two deformed steel (H- and T-) fibers, two fiber volume, (1% and 1.5 %) contents and two matrixes (Ma and Mb for 56 and 81 MPa compressive strength) were investigated. The matrix compositions are provided in Table 1 while the properties of fibers are given in Table 2.

Sand, cement, fly ash and silica fume (for Mb only) were first mixed in dry condition for 3 min. And, water was added to the dry mixture slowly three times with 2 min intervals. Then, super-plasticizer was gradually added until the mortar mixture showed adequate workability and viscosity for uniform fiber distribution. Fibers were distributed by hand during the mixing. A visual attention of the mortar mixture during adding fiber should be paid to ensure the uniform distribution of fibers in the mixture. It should be noticed that excessive water or super-plasticizer would lead to the segregation of fibers, and, as a result, the mechanical resistance of HPFRCCs would decrease. Thus, the workability and viscosity of mortar mixture was strictly controlled by investigating the slump flow test to avoid fibers' gravitation or segregation. The slump flow of HPFRCCs with steel fibers was kept as about 600 mm; and there was no visible segregation of fibers. The mortar mixture with fibers was then poured into molds. The specimens after casting were covered by plastic sheet and stored in a laboratory at room temperature. After 24 h, all specimens were demolded and placed in a water tank with temperature of $23 \pm 2^\circ\text{C}$ for curing in additional 14 days. Finally, the specimens were removed and dried in the laboratory for 3 days before spraying three layers of thin polyurethane for cracks detection. All specimens stored in laboratory at room temperature about 3 months until testing.

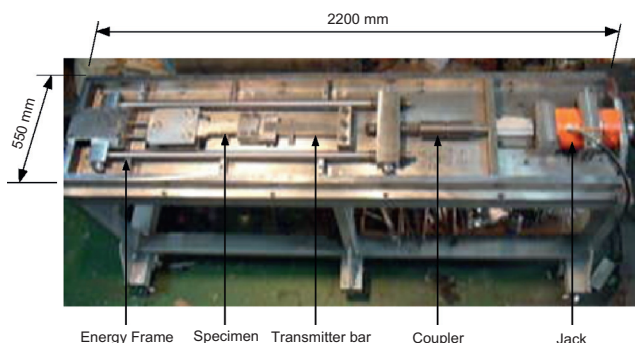


Fig. 2. Strain Energy Frame Impact Machine (SEFIM).

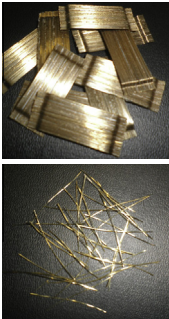
Table 1

Matrix composition by weight ratio and compressive strength.

Matrix	Cement (Type III)	Fly ash	Silica sand	Silica fume	Super-plasticizer	Water	f'_c (MPa)
Ma	1.00	0.15	1.00	–	0.009	0.35	56
Mb	0.80	0.20	1.00	0.07	0.04	0.26	81

Table 2

Properties of fibers.

Fiber type	Diameter (mm)	Length (mm)	Density (g/cc)	Tensile strength (MPa)	Elastic modulus (GPa)	Images
Hooked	0.375	30	7.9	2311	200	
Twisted	0.300 ^a	30	7.9	2428 ^b	200	

^a Equivalent diameter.^b Tensile strength of the fiber after twisting.**Table 3**

Test matrix.

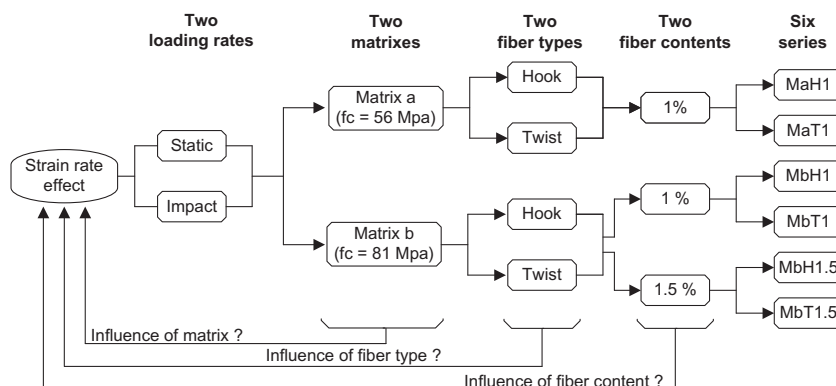
Matrix	Fiber content	Notation	Number of specimens	
			Static rate (0.000167 s ⁻¹)	Higher rates (10–40 s ⁻¹)
Ma	H-fiber 1%	MaH1	4 ea	4 ea
	T-fiber 1%	MaT1	4 ea	4 ea
Mb	H-fiber 1%	MbH1	4 ea	4 ea
	T-fiber 1%	MbT1	4 ea	4 ea
	H-fiber 1.5%	MbH1.5	4 ea	4 ea
	T-fiber 1.5%	MbT1.5	4 ea	4 ea

by two layers of steel wire mesh to prevent from failure of outside gauge length. Since the length of fiber is 30 mm while the thickness and width of the specimen is 25 mm and 50 mm, respectively, the effect of fiber distribution should be considered in the analysis of test results. To minimize the effect, two following procedures were applied: (1) the workability and viscosity of mortar mixture was strictly controlled to prevent fibers from segregation and sinking during mixing as mention above; (2) the mortar mixture was also placed in molds little by little from one end to the other end with two layers during casting. All specimens for both static and impact tests were tested with the same gauge length of 100 mm. Since the specimens were casted on the molds with gauge length of 175 mm, not 100 mm, thus the wire meshes of one end were extended longer than those of other end as shown in Fig. 4. The identical of geometry for both static and impact tests eliminated potential size effect and fiber distribution effect on the estimation of the strain rate effects.

For static tests, the elongation of specimens during the test was measured through two LVDTs as shown in Fig. 4. The strain history was obtained by analyzing the signals from the attached LVDTs. The stress history was measured from the load cell located on

2.2. Test set-up and procedure

The test set-up and geometry of specimens were described in Figs. 4 and 5 for static and impact test, respectively. The specimens have a cross section of 25 × 50 mm and two bell-shaped reinforced

**Fig. 3.** Details of the experimental program.

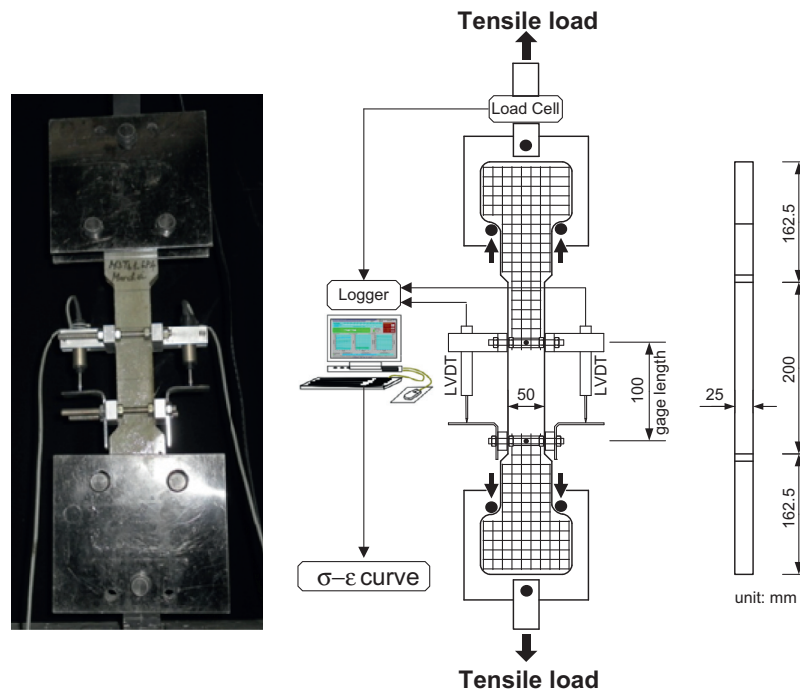


Fig. 4. Test set-up and geometry of specimen for static test.

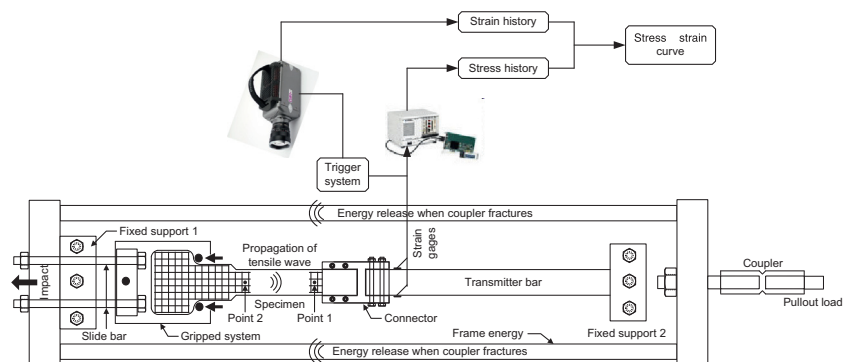
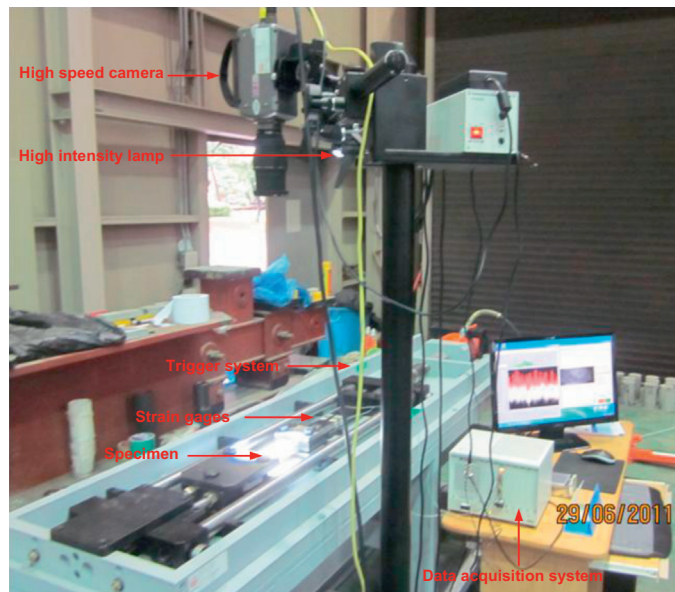


Fig. 5. Test set-up and geometry of specimen for impact test.

the top of the specimen. Then, the stress versus strain response was achieved by combining the stress and strain histories.

For impact tests, to obtain stress histories propagated from the tensile specimen, one end of bell-shaped specimen was cut off and then connected directly to transmitter bar by a connector as described in Fig. 5. The remaining bell-shaped end was gripped by a hinge system connected to energy frame by two slide-bars. The energy frame was prevented from movement by a fixed support 1 at one side while the other side was connected to a hydraulic jack through a coupler. Once the jack was pumped, the coupler would be pulled out and the strain energy would be stored in frame. Until reaching the maximum capacity, the coupler was suddenly broken leading to the stored strain energy in frame released rapidly. Such rapidly released strain energy, in turn, made the frame impact to both ends of slide bars. Since the transmitter bar was prevented from movement by a fixed support 2, an impact event occurred at the ends of two slide-bars would produce a high rate tensile stress wave propagated through the hinge grip to the specimen and eventually failed specimen. The stress history of specimen was obtained by two strain gauges attached at both sides of the transmitter bar while the strain history was measured through the elongation of specimen by monitoring the movement of two marked points with a gauge length of 100 mm using high speed camera as shown in Fig. 5. Based on the stress and strain histories of specimen, the stress versus strain response of specimen could be established.

3. Test results

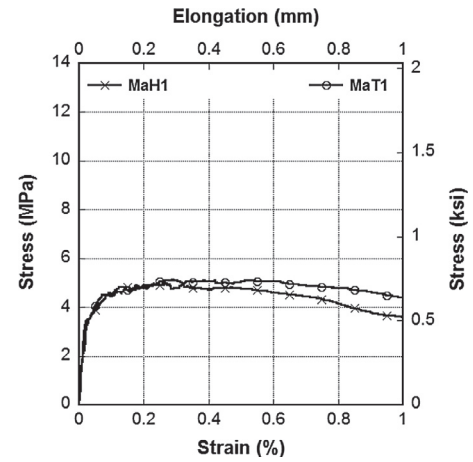
To evaluate the direct tensile behavior of HPFRCCs at high strain rates and their different rate sensitivity, four parameters are analyzed as follows: (1) p_c , the post cracking strength, is the peak stress value in the stress versus strain curve, (2) p_c , the strain capacity, is the strain at peak stress (3) the peak toughness T_{pc} , the absorbed energy per unit volume of material, is defined as the area under the tensile stress versus strain curve until post cracking strength point, and (4) dynamic increase factor (DIF) is the ratio between dynamic and static response for above three parameters.

3.1. Static test results

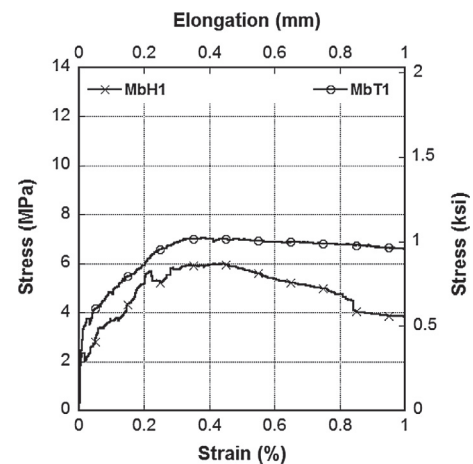
Fig. 6 shows the tensile stress versus strain curves of six series, composed of Ma and Mb matrixes reinforced by H- and T- fibers with volume content 1%, notated as H1 and T1, and 1.5 %, notated as H1.5 and T1.5, at static rate equivalent to 0.000167 s^{-1} . All these curves shown in Fig. 6 are the averaged ones at least from three test results. The averaged tensile parameters are provided in Table 4.

All series of HPFRCCs produced multiple cracking behaviors as shown in Fig. 7. In general, both fibers were effective in developing tensile strain hardening response as shown in Fig. 6, and T-fiber reinforced specimens produced higher number of multiple micro cracks than H-fiber reinforced specimens regardless of matrix type and fiber volume content. In addition, the specimens with higher fiber volume content (1.5%) generated more number of multiple cracks than those with lower fiber volume content (1%).

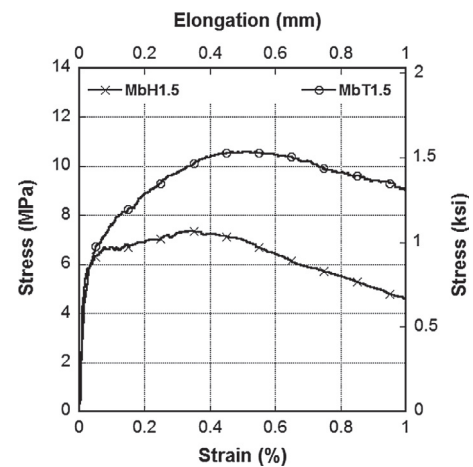
In particular, T-fiber produced higher tensile strength and energy absorption capacity for both matrixes Ma and Mb. The post cracking strength of HPFRCCs reinforced by two fiber types in lower strength matrix Ma (5.1 and 5.0 MPa for MaT1 and MaH1) was almost identical while that in higher strength matrix Mb (7.1 and 6.0 MPa for MbT1 and MbH1) was significantly different according to the types of fiber especially for 1.5% fiber volume contents (11.8 MPa and 7.4 MPa for MbT1.5 and MbH1.5). The strain capacities were also different according to the fiber types and matrix.



(a) MaH1 and MaT1



(b) MbH1 and MbT1



(c) MbH1.5 and MbT1.5

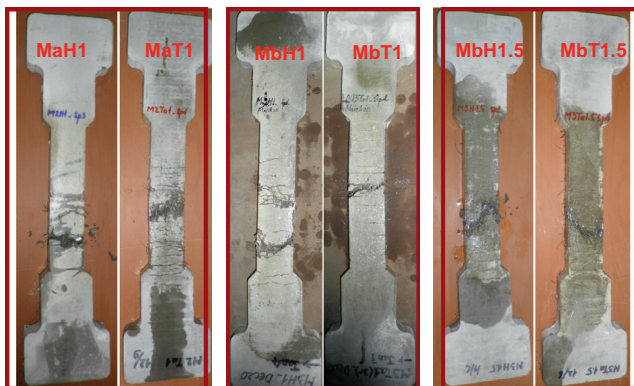
Fig. 6. Tensile stress versus strain curves of specimens tested at static rate.

The strain capacities of MaT1 and MaH1 were 0.29% and 0.27%, respectively while those of MbT1 and MbH1 were 0.39% and 0.45%. And, those of MbT1.5 and MbH1.5 were 0.49% and 0.34%, respectively. As the strength of matrix and fiber volume content increased, the strain capacity for T- fiber reinforced HPFRCCs was enhanced while there was no clear tendency for H- fiber.

Table 4

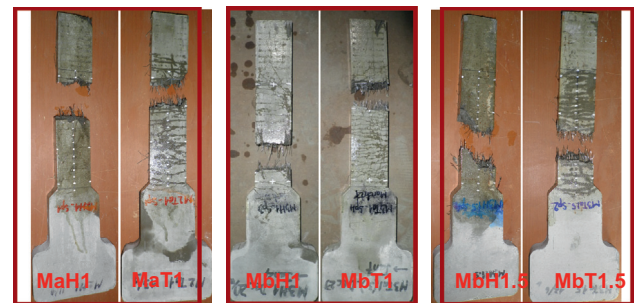
Test data.

Test series	Strain rate	Rate (s^{-1})	Spe.	Post cracking strength		Strain capacity		Peak toughness	
				MPa	DIF	%	DIF	kJ/m^3	DIF
MaH1	Static	0.000167	Ave.	5.0	1	0.27	1	11.7	1
	High rate	16.8	Sp1	15.2	3.1	0.92	3.5	122.5	10.5
		10.4	Sp2	12.3	2.5	0.67	2.5	40.6	3.5
		11.2	Sp3	23.2	4.7	0.82	3.0	46.5	4.0
		Average		16.9	3.4	0.80	3.0	69.9	6.0
MaT1	Static	0.000167	Ave.	5.1	1	0.29	1	12.9	1
	High rate	16.2	Sp1	23.8	4.6	0.54	2.0	40.0	3.1
		12.3	Sp2	15.1	2.9	0.86	3.2	75.7	5.9
		7.6	Sp3	18.6	3.6	0.96	3.6	121.1	9.4
		Average		19.2	3.7	0.79	2.9	78.9	6.1
MbH1	Static	0.000167	Ave.	6.0	1	0.45	1	21.2	1
	High rate	19.2	Sp1	20.2	3.4	1.40	3.1	139.4	6.6
		11.2	Sp2	24.7	4.1	1.48	3.3	145.3	6.9
		23.3	Sp3	18.9	3.1	1.74	3.9	210.0	9.9
		Average		21.3	3.6	1.54	3.5	164.9	8.2
MbT1	Static	0.000167	Ave.	7.0	1	0.39	1	22.1	1
	High rate	13.5	Sp1	17.4	2.5	1.34	3.4	110.5	5.0
		21.3	Sp2	25.5	3.6	1.42	3.6	190.8	8.6
		28.7	Sp3	18.9	2.7	1.94	5.0	269.2	12.2
		Average		20.6	2.9	1.56	4.0	190.2	8.6
MbH1.5	Static	0.000167	Ave.	7.4	1	0.34	1	22.6	1
	High rate	9.3	Sp1	19.2	2.6	0.49	1.4	58.5	2.6
		17.7	Sp2	16.5	2.3	1.23	3.6	155.1	6.9
		15.6	Sp3	29.7	4.0	1.03	3.0	169.8	7.5
		Average		21.8	3.0	0.92	2.7	130.9	5.7
MbT1.5	Static	0.000167	Ave.	11.8	1	0.49	1	42.2	1
	High rate	17.3	Sp1	25.6	2.2	1.57	3.2	128.3	3.0
		16.7	Sp2	35.1	3.0	1.19	2.4	128.0	3.0
		14.4	Sp3	38.2	3.3	0.94	1.9	117.1	2.8
		Average		33.0	2.8	1.23	2.5	124.5	3.0

**Fig. 7.** Cracking behavior of specimens tested at static rate.

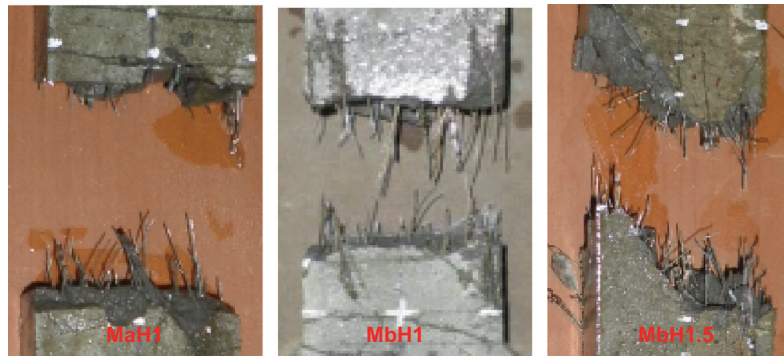
3.2. Impact test results

Fig. 8 shows the photos of six series of specimens tested at higher strain rates using SEFIM while Fig. 7 provides the photos of specimens tested at static rates. As shown in Figs. 7 and 8, there is clear difference in their cracking pattern between static and impact tests. First, the specimens tested at high strain rates produced more number of micro cracks than those tested at static rate. Second, the specimens tested at high strain rates showed localized major cracks perpendicular to the loading direction as shown in Fig. 8 while most of them tested at static rate produced the inclined localized major crack as shown in Fig. 7. This observation demonstrated that the specimens tested at higher rates were under

**Fig. 8.** Cracking behavior of specimens tested at high strain rates using the SEFIM.

uniaxial tensile condition and generated higher energy absorption capacity than at static rate. In addition, the fibers at the localized fractured section of specimens were generally pulled out from the matrix without fiber breakage. It is also noticeable that the end hook of H-fibers were straightened for the specimens tested at high strain rates as shown in Fig. 9a unlike the specimens tested at static rate as shown in Fig. 9b. The fibers were pulled-out at the fractured section; and, this observation supported the idea that the localized final failure of HPFRCCs was dominated by the debonding and pullout mode of fibers at the interface. Thus, the interfacial debonding and fiber pullout at the interface between fiber and matrix is a key parameter influencing the tensile behavior of HPFRCCs at high strain rates.

The strain rates generated using SEFIM vary between $7.6 s^{-1}$ and $28.7 s^{-1}$ as provided in Table 4 although the same couplers were used for tests. The different strain rates may be from the



(a) The fibers of H-specimens almost were pulled out and become straight in impact test



(b) The fibers of H-specimens almost still remain the hooks in static test

Fig. 9. The fibers of H-specimens almost were pulled out and become straight.

slight difference in the depth of notch in the couplers or the nature of un-homogeneous characteristics of composites. Fig. 10 provides the tensile stress versus strain curves in sample for all series. The word “sample” means the curves were plotted with respect to identical-rate-pairs. Before building the curves, a process of synchronization the stress history and strain history should be carried out. Details of this technique could be found in [14].

As shown in Fig. 10, it is important to notice that all series of HPFRCCs maintained the typical strain hardening behavior with high ductility and energy absorption capacity at higher strain rates. HPFRCCs at higher strain rates showed favorable strain rate effects, i.e., higher post cracking strength, strain capacity and energy absorption capacity although the enhancement of them were quite different according to the type of fibers, fiber volume contents and matrixes. These issues will be discussed in detail below.

4. Discussion

4.1. Effect of fiber type on rate sensitivity of HPFRCC

Fig. 11 shows the effect of fiber type on strain rate sensitivity of HPFRCCs. The effects of fiber type on the change of post cracking strength, strain capacity and peak toughness according to the applied strain rates were provided in Fig. 11a, b, and c, respectively. To compare the strain rate sensitivity, DIFs for each parameter were calculated and plotted as dots according to corresponding strain rates as shown in Fig. 11.

Both H- and T-fibers clearly produced strong rate sensitivity for all parameters including post cracking strength, strain capacity and peak toughness. For example, the post cracking strength and the strain capacity were enhanced around 3 times as shown in Fig. 11a and b, while the peak toughness was enhanced around 6 times as shown in Fig. 11c. Until seismic strain rate, HPFRCCs with T-fibers were reported as sensitive to strain rate, i.e., the DIF for post cracking strength was around 1.7 for MaT1, while the HPFRCCs with H-fibers were not [7]. The higher strain rates than

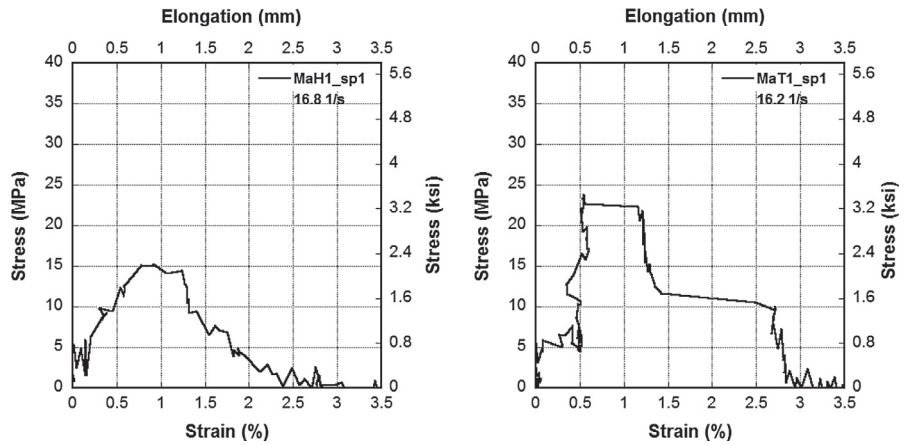
seismic rate not only activated the rate sensitivity of HPFRCC with H- fibers but also increased the rate-sensitivity of the HPFRCCs with both H- and T-fibers from 1.7 to 3.

The effect of fiber type on the rate sensitivity of HPFRCC could be observed from the test result of Mb1 series only. HPFRCCs with H-fibers produced higher rate sensitivity for post cracking strength, than those with T-fibers, but lower rate sensitivity for both strain capacity and peak toughness. For comparison, the average values of DIFs were provided in Table 4. The DIF (3.6) of post cracking strength for MbH1 is higher than that (2.9) for MbT1, while the DIF (3.5) of strain capacity for MbH1 is smaller than that (4.0) for MbT1. It should be also noticed that, the specimens with H-fibers produce higher DIF for post cracking strength than the specimens with T-fibers in Mb matrix, while DIF for post cracking strength of them are converse, in Ma matrix, i.e., 3.4 for MaH1 is smaller 3.7 for MaT1.

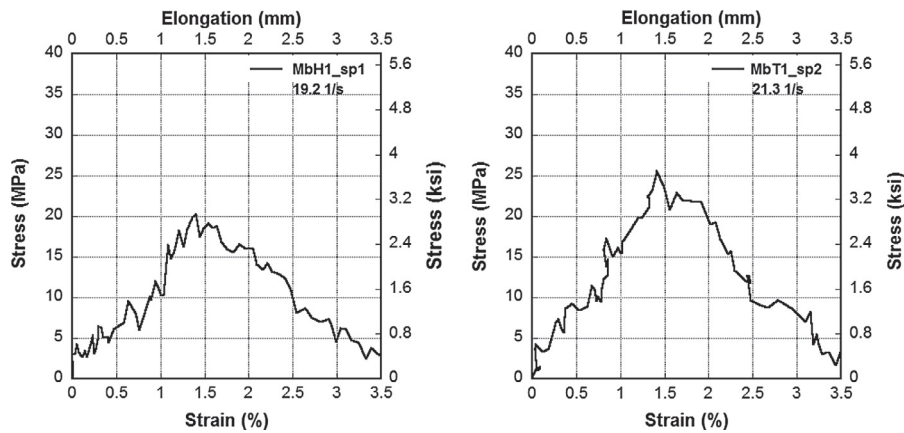
In summary, H-fibers produced strong rate sensitivity for post cracking strength at high strain rate while they did not produce any rate sensitivity until seismic rate. In contrast, T-fibers not only showed noticeable rate sensitivity at seismic rate, but also produced stronger rate sensitivity at high strain rates. And, as the strength of matrix increased from 56 MPa (Ma) to 81 MPa (Mb), the rate sensitivity for post cracking strength of H-specimen increased while that of T-specimen decreased. For peak toughness, except the case of MbH1.5 and MbT1.5, both H- and T-fibers showed similar rate sensitivity although they were different according to matrix type, as shown in Fig. 11c.

4.2. Effect of fiber volume content on rate-sensitivity of HPFRCC

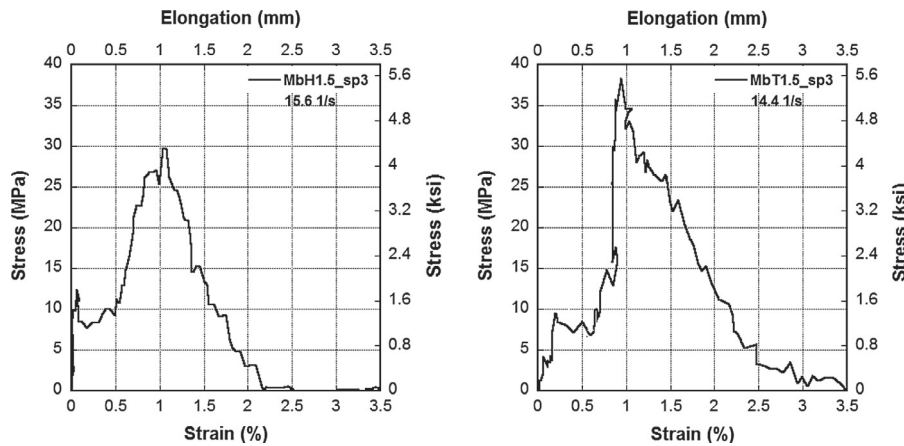
The effect of fiber volume contents on the rate sensitivity of HPFRCCs is shown in Fig. 12a, b and c for post cracking strength, strain capacity and peak toughness, respectively. Black dots (1.0%) are located in higher position in Fig. 12 than white dots (1.5%): HPFRCCs with lower fiber volume content, regardless of fiber type, produced higher rate sensitivity for all three parameters



(a) MaH1 and MaT1



(b) MbH1 and MbT1



(c) MbH1.5 and MbT1.5

Fig. 10. Tensile behavior of HPFRCCs at high strain rate.

as shown in Fig. 12. As the volume contents of fiber increased from 1.0% to 1.5%, the rate sensitivity for post cracking strength decreased as illustrated in Fig. 12a: the DIFs for the post cracking strength of HPFRCCs with H-fibers are 3.6 and 3.0 for 1.0% and 1.5% fiber volume contents, respectively while those of HPFRCCs with T-fibers are 2.9 and 2.8 for 1.0% and 1.5% fiber volume contents, respectively. The DIFs for the strain capacity also significantly decreased from 4.0 to 2.5 for T-fibers and from 3.5 to 2.7 for H-fibers, respectively, as shown in Fig. 12b as the fiber volume

content increased from 1.0% to 1.5%. The effect of fiber content on DIFs for the peak toughness of HPFRCCs was also clearly demonstrated in Fig. 12c: 8.6 for MbT1, 3.0 for MbT1.5, 8.2 for MbH1 and 5.7 for MbH1.5, respectively. Same tendency, at high strain rates, of lower rate-sensitivity at higher fiber volume contents was reported by Kim et al. [7]. And, the fiber group effect can be used to explain the lower rate sensitivity at higher fiber volume contents. For static case, the group effect was pointed out by Naaman [15]: “the pullout capacity of group of randomly oriented

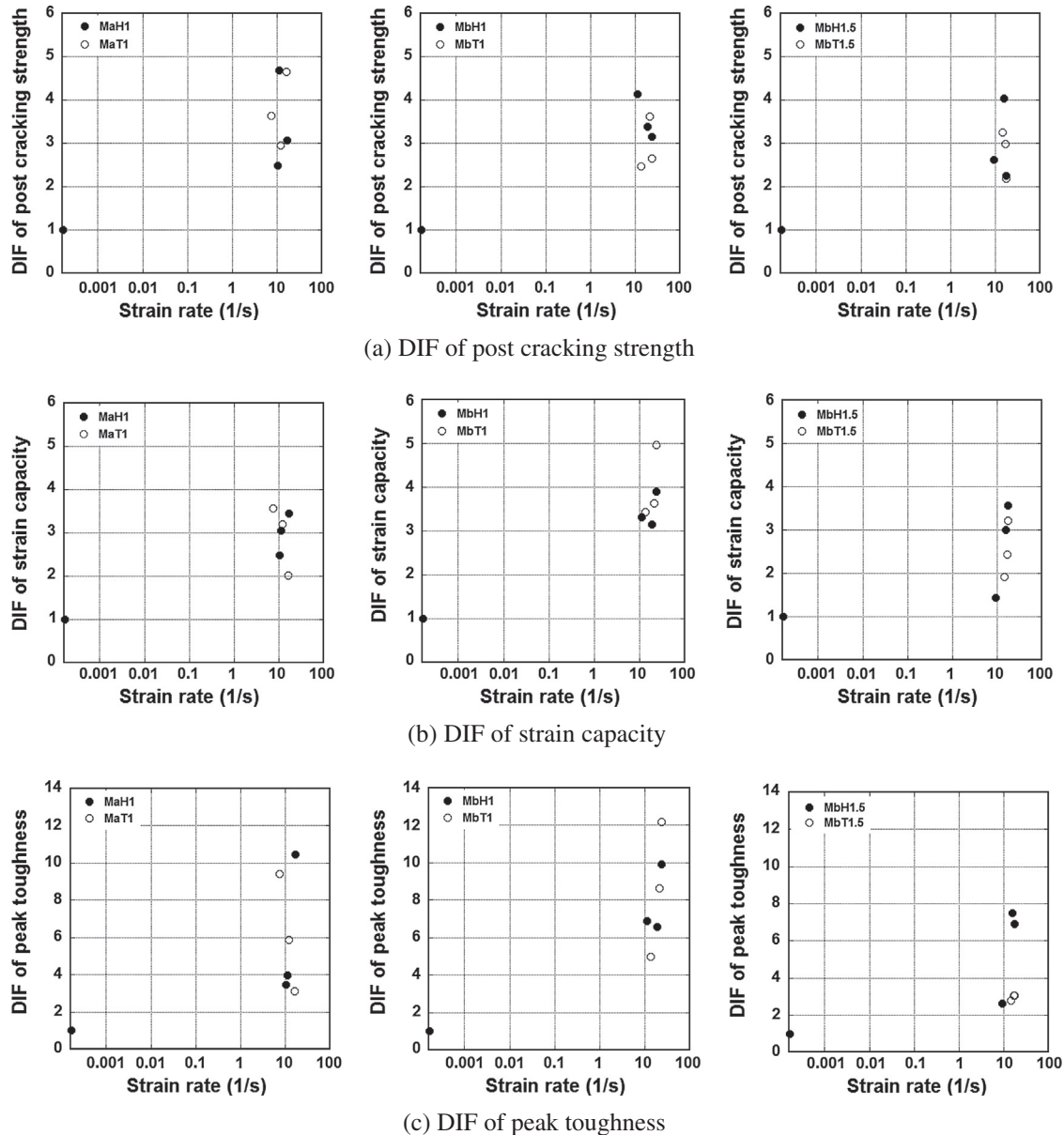


Fig. 11. Fiber type effect on strain rate sensitivity of HPFRCC.

fibers decreases drastically when the number of fibers pulling out from the same area increases". It might be explained identically in the impact case. The group effect occurs when a group of fibers interact together during pull out, is not as rate sensitive as single fiber pull out. In addition, once the number of fiber is too much, the amount of matrix surrounding the fiber will not be enough to maintain the interfacial bonding as strong as in the single pull-out case, which could lead to dilute or eliminate rate sensitivity.

4.3. Effect of matrix type on rate-sensitivity of HPFRCC

Effect of matrix strength on DIFs for post cracking strength, strain capacity and peak toughness is described in Fig. 13a, b and c, respectively. All graphs, except the figure for MaT1 and MbT1 in Fig. 13a for the post cracking strength of HPFRCCs with 1% T-fibers, show that higher strength matrix (Mb) are above lower strength matrix (Ma). All series, except the post cracking strength of HPFRCC reinforced with 1% T-fibers, produced higher enhancement in the higher strength matrix (Mb), at high strain rates, than

in the lower strength matrix (Ma). In other words, the higher strength matrix (Mb) produced more sensitive response to the applied strain rates.

HPFRCC contains many microdefects including interfacial transition zone between fiber and matrix. These defects grow during loading and the failure only occurs when the defects reach to certain critical size. The defects at that time, also called micro-cracks, will extend to zones that have the lowest tensile strength and bond strength. This process requires a period of time. In the case of high rate loading, where failure occurs within a very short time, only around 3 ms; thus, the defects do not have enough time to seek the zones with least resistance, instead, defects will propagate to high strength zone which requires more energy. The impact resistance, therefore, must increase as the rate of loading increases. The enhancement of impact resistance could also be explained as in [16] for concrete and mortar: under static tensile loading conditions, "the growing cracks have time to choose and develop along the path of least energy requirement, i.e., around aggregate particles and through the weakest zones of the matrix" while under

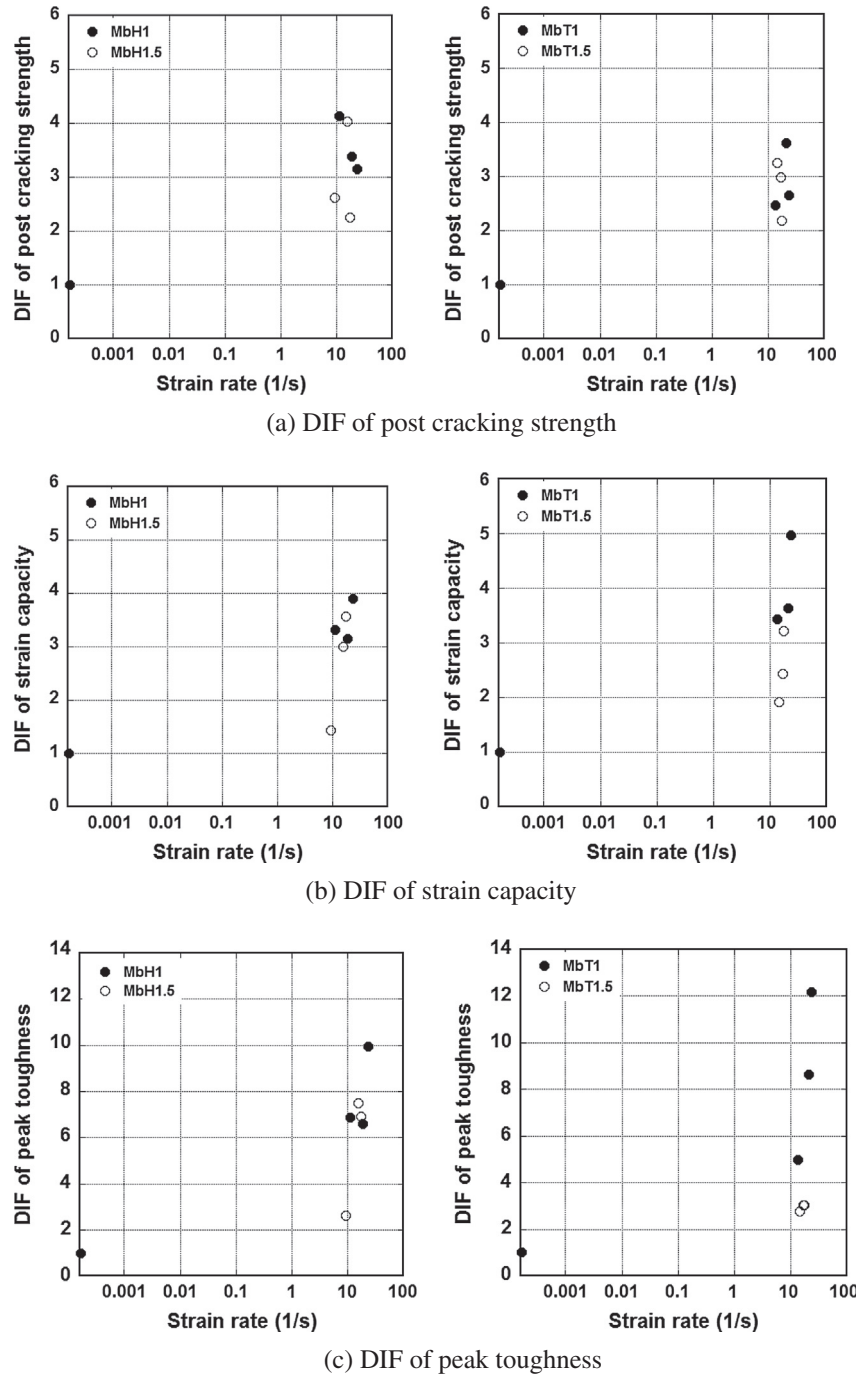


Fig. 12. Influence of fiber contents on strain rate sensitivity of HPFRCC.

impact tensile loading conditions, “cracks are forced to develop along shorter paths of higher resistance through stronger matrix zones and some aggregate particles leading to the higher impact tensile strength”.

In addition, higher strength matrix, generally containing smaller size defects and interfacial transition zone between fiber and matrix [17], might require longer time for those defects or micro cracks growing to critical size of crack propagation than lower strength matrix. Therefore, the higher rate sensitivity of HPFRCCs observed in high strength mortar matrix is due to the smaller size of defects or micro cracks inside. It should be noticed that the explanation is just authors' hypothesis. More experiments should be carried out to clarify this view point.

However, the HPFRCC with T-fibers produced lower rate sensitivity for post cracking strength in higher strength matrix (Mb). The reason for higher rate sensitivity of post cracking strength in lower strength matrix (Ma) may be from the different pullout behavior as shown in Fig. 14 [18]. Fig. 14 shows that, after reaching to initiation of mechanical bond (IMB), the pullout load further increases in Ma while it decreases in Mb. The increasing slope provides more mechanical interaction between fiber and matrix during pullout and time for complete interfacial damage or debonding. Since the bond between fiber and matrix is the key factor leading to the dynamical resistance enhancement at high rate loading [14], thus, for T-fiber, this different mechanism maybe a reason for higher rate sensitivity for the

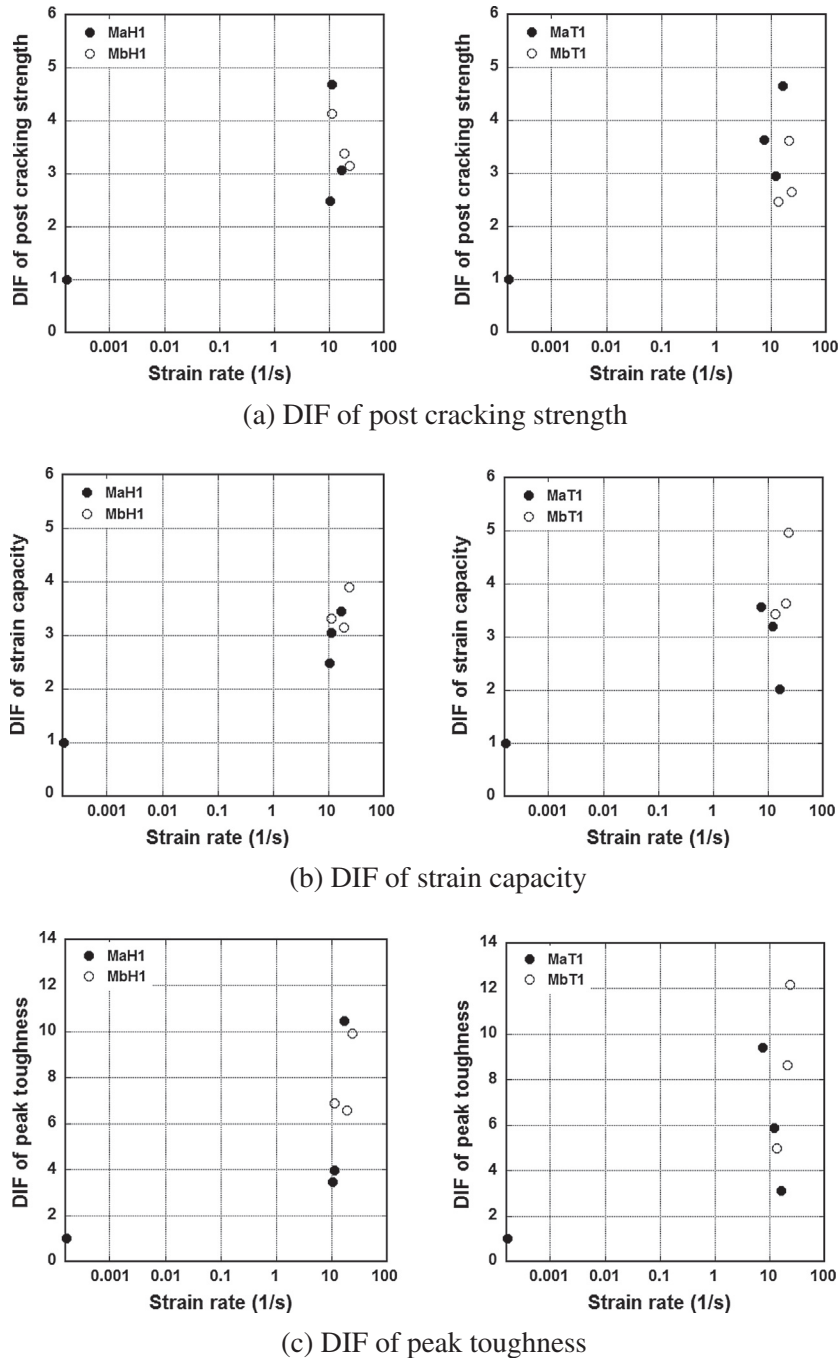


Fig. 13. Influence of matrix types on strain rate sensitivity of HPFRCC.

post cracking strength of HPFRCC with lower strength matrix, Ma, than the higher one, Mb.

4.4. The role of fiber type, fiber content and matrix type on direct tensile impact behavior of HPFRCC

Effect of fiber type, fiber content and matrix strength on direct tensile impact resistance and on rate sensitivity of HPFRCC is summarized in Figs. 15 and 16, respectively. The values in the figures are the average values as provided in Table 4. It should be noticed that, the comparison here is relative since these average values obtained from the various strain rates between 7.6 s^{-1} and 28.7 s^{-1} .

Fig. 15 shows the values of T-fiber are almost higher than the ones of H-fiber, proving that T-fiber is more advantageous than

H-fiber at high strain rate. Fig. 15 also shows trend for tensile properties at higher strain rates under impact. For example, an increasing in compressive strength of matrix from 56 MPa (Ma) to 81 MPa (Mb), results in an increase of all properties including the tensile strength σ_{pc} , strain capacity ε_{pc} and peak toughness T_{pc} of composite, as shown in Fig. 15a. Meanwhile, in Fig. 15b, an increasing in fiber volume from 1% to 1.5% results in an increase of the tensile strength only, but decrease of strain capacity as well as peak toughness. This observation demonstrates that the strength of matrix plays more major role than the fiber content in improving the impact resistance of HPFRCCs. Similar conclusion about the role of matrix strength comparing to fiber content in rate sensitivity of HPFRCC is also drawn from Fig. 16. An increasing in compressive strength of matrix from 56 MPa (Ma) to 81 MPa (Mb), results in

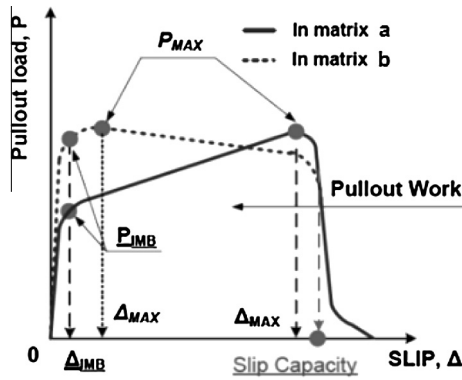


Fig. 14. Pseudo-static slip-hardening fiber pullout behavior [14].

an increase of DIF of strain capacity and DIF of peak toughness, as shown in Fig. 16a; while, in Fig. 16b, an increasing in fiber volume from 1% to 1.5% results in a decrease of all properties including DIF of post cracking strength, DIF of strain capacity and DIF of peak toughness.

Based on this result, a goal driven optimization of mix proportion for HPFRCC can be achieved through composing appropriately three main components including fiber type, fiber content and matrix strength. For example, to achieve a high impact resistance of all properties including post cracking strength, strain capacity and peak toughness, the higher strength matrix Mb and T-fiber are chosen (Fig. 15a). Then, if the requirement of post cracking strength is priority for this type of HPFRCC, 1.5% of volume content is chosen as shown in the graph of post cracking strength of Fig. 15b. Conversely, if the requirement of strain capacity and peak toughness is priority, 1% volume content is chosen as shown in the two remaining graphs of Fig. 15b.

4.5. The role of interfacial bonding between fiber and matrix on direct tensile impact behavior of HPFRCC

Under static loading conditions, Naaman [1] suggested the following equation to predict the post cracking strength:

$$\sigma_{pc} = \lambda \tau V_f (L_f / d_f) \quad (1)$$

where V_f is fiber volume fraction, L_f is fiber length, d_f is fiber diameter, L_f/d_f is fiber aspect ratio, τ is bond strength, λ is factor equal to the product of several coefficients for considering average pullout length, group reduction, orientation effect.

Note that the post cracking strength σ_{pc} (Eq. (1)) is a function of fiber volume fraction V_f , fiber aspect ratio L_f/d_f and bond strength τ between fiber and matrix. The contribution of matrix, in this case, is hidden in bond strength τ . The higher strength of matrix, the higher strength of interfacial bonding, leading to the higher post cracking strength. Although this equation is used in static case, but at least it provided more information on the mechanical understanding and pointed out that the post cracking strength depending on three components including matrix, fiber and the interfacial bonding between them not only in static case but also in impact one.

The role of interfacial bonding between fiber and matrix was pointed out in [14] based on the observed rate sensitive responses of mortar and HPFRCCs with 1% in content of T and H fibers. The enhancement of tensile strength for mortar matrix, a component of HPFRCC, was only 30% while the enhancement of tensile strength for HPFRCCs was around ten times larger. The other component of HPFRCC is steel fiber. Nicholas [19] reported that there was not much enhancement of steel strength, around 15%, under tensile loading rate of 20 s^{-1} . Thus, the main source for the rate sensitivity behavior of HPFRCC is the remained component, i.e., the interfacial bond strength between fiber and matrix.

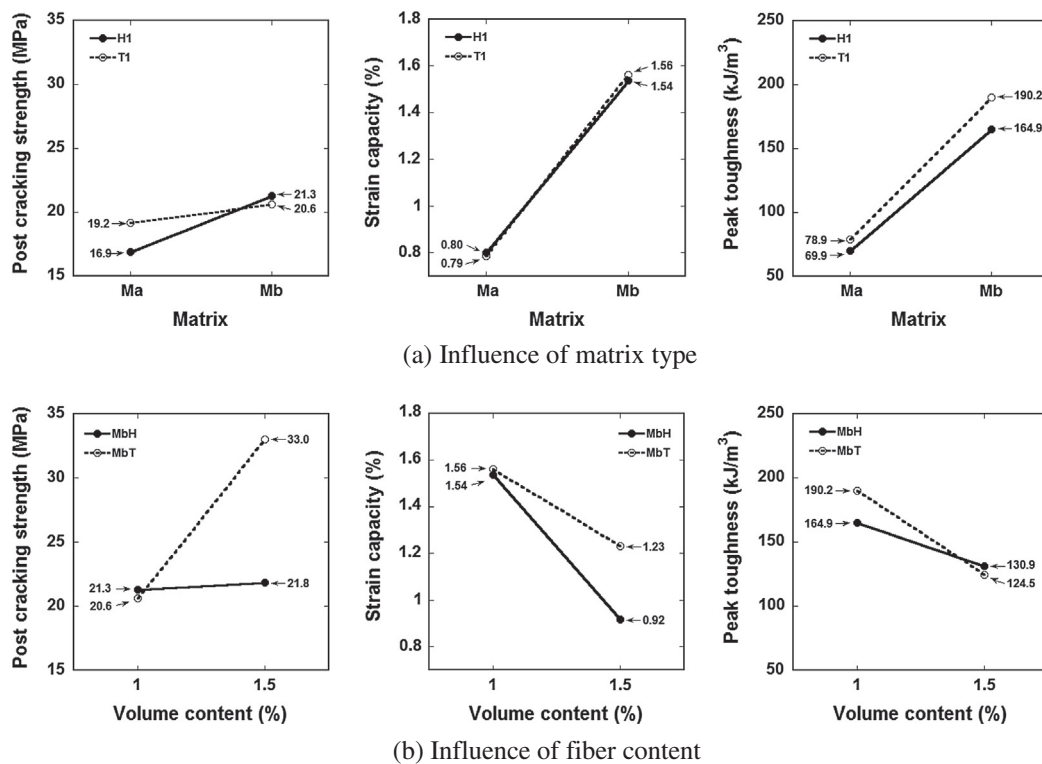


Fig. 15. Influence of matrix types and fiber contents on impact resistance of HPFRCCs.

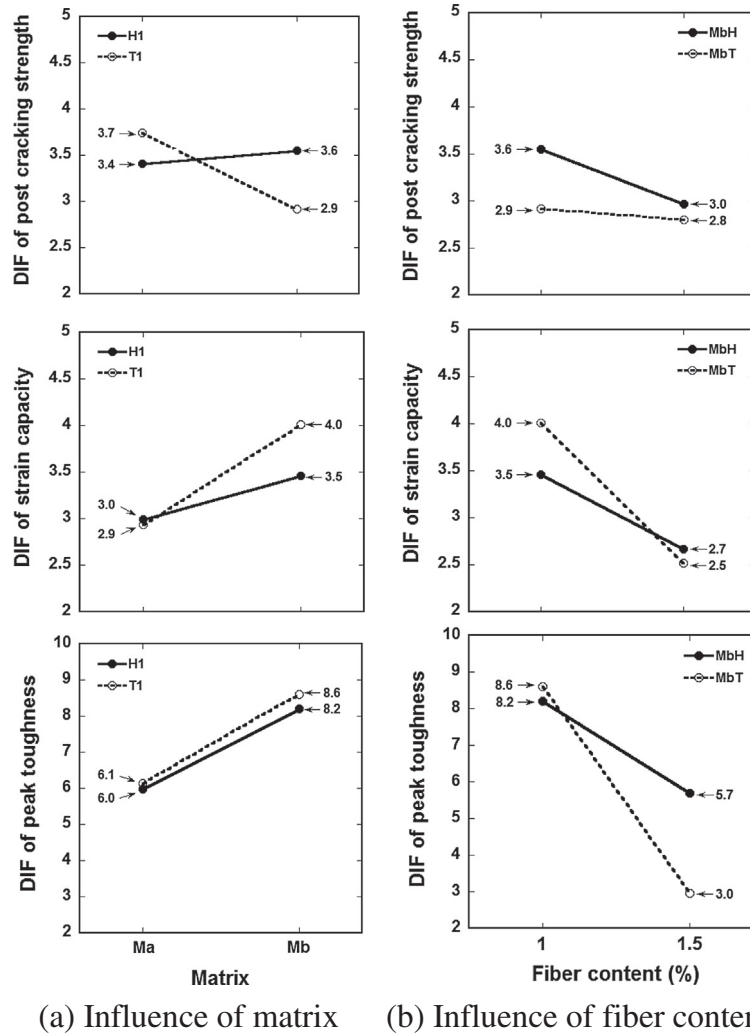


Fig. 16. Influence of fiber types, fiber contents and matrix types on rate-sensitivity of HPFRCC.

The inertial effect of matrix surrounding deformed steel fiber is thought to be a reason leading to the enhancement of interfacial bond strength. An acceleration of the material particles in the mortar matrix surrounding fiber will occur when the mortar matrix is rapidly loaded at high strain rates. This acceleration results in the additional clamping pressure on the surface of fiber due to inertial effect, making the interfacial bond strength stronger at high strain rates. Thus, the bond strength is the key to the strong rate sensitivity, and, the improved interfacial bond strength at high strain rates would increase the post cracking strength.

4.6. Predicting DIF of post cracking strength for HPFRCC

Both tensile and compressive strengths of concrete-like materials (e.g. mortar, concrete and geo-materials) increase as strain rate increases [20,21]. To predict a dynamic strength at a given strain rate ranging from 3×10^{-6} to 300 s^{-1} , the CEB formulation [22] has been commonly used.

The correlation between the tensile strength of concrete and strain rate is described using two lines in log scale figure as shown in Fig. 17. The slope of second line suddenly increases at the strain rate of 30 s^{-1} as described in the equation, namely CEB formulation. However, “the available data at high strain rates seems to support that the change in slope occurs close to 1 s^{-1} instead of at 30 s^{-1} as assumed by CEB”, and, “it seems appropriate to assume

the quasi-static strain rate at $1 \times 10^{-6} \text{ s}^{-1}$ ” [23]. Thus, Malvar and Ross [23] modified CEB formulation by fitting against the available data, and the proposed formulation then becomes:

$$DIF_{ft} = \left(\frac{\dot{\varepsilon}}{\dot{\varepsilon}_s} \right)^{\delta} \quad \text{for } \dot{\varepsilon} \leq 1 \text{ s}^{-1} \quad (2)$$

$$DIF_{ft} = \beta \left(\frac{\dot{\varepsilon}}{\dot{\varepsilon}_s} \right)^{1/3} \quad \text{for } \dot{\varepsilon} > 1 \text{ s}^{-1} \quad (3)$$

where DIF_{ft} is dynamic tensile strength at $\dot{\varepsilon}$; $\dot{\varepsilon}$ is the strain rate in the range of 10^{-6} to 160 s^{-1} ; $\dot{\varepsilon}_s$ is static strain rate, 10^{-6} s^{-1} ; $\log \beta = 6\delta - 2$; $\delta = 1/(1 + 8f'_c/f'_{co})$; f'_c is static compression strength; and f'_{co} is a constant equal to 10 MPa. The question is whether this equation can be applied for the HPFRCC? Is it possible to add the effect of fiber type, fiber content and matrix type in the previous equations?

Fig. 17, where the DIF versus strain rate from static to high strain rate of four series MaH1, MaT1, MbH1 and MbT1 are plotted together with the Malvar and Ross' curves, provides the positive answer of the first question. The data plotted in the figure included not only the data in Table 4 at high strain rate, but also the data of Kim et al. [7] at seismic strain rate. In log-log scale, the Malvar and Ross' curve displays a two-segment trend-line with a knee located at seismic strain rate, 1 s^{-1} . Although the available data is lack at

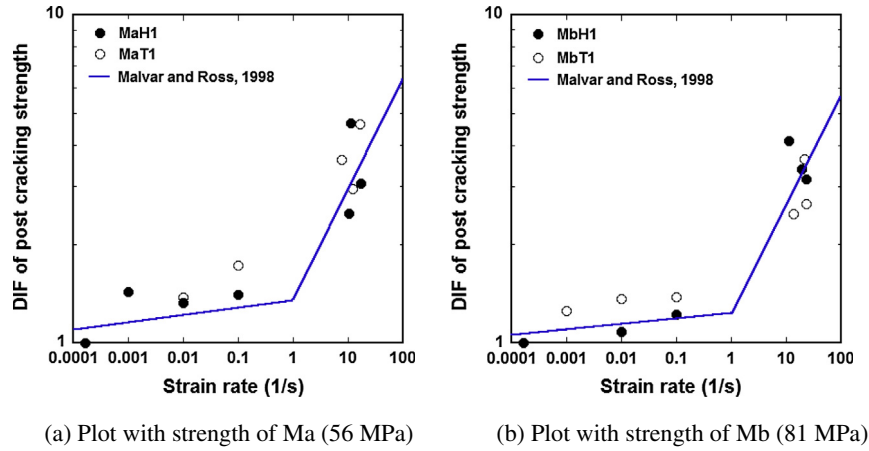


Fig. 17. Malvar and Ross' curve to predict DIF of strength for concrete.

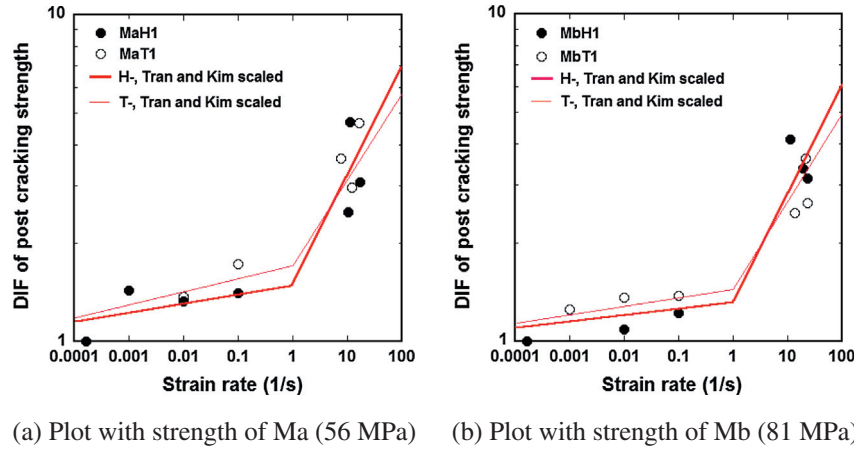


Fig. 18. Proposed formulation to predict DIF of post cracking strength for HPFRCCs.

1 s^{-1} , the distribution of the dots seems to follow the Malvar and Ross' curves. However, the curves do not reflect the difference of the fiber type in HPFRCC. Thus, an appropriate modification to predict DIF of post cracking strength for HPFRCCs with considering the fiber type and matrix type effects is necessary.

Three new parameters, namely m , h , k , in which m is a parameter describing the difference of strength between concrete and HPFRCC, h and k are parameter describing effect of fiber type, were added to modify Malvar and Ross' formulation. There are two purposes of introducing parameters: (1) to specify the relationship of inheritance between traditional concrete and HPFRCC, (2) to open the ability of application the research successes of concrete into HPFRCC, such as modification and application of available concrete models in commercial program to simulate HPFRCC structures. The new formulation as follows:

$$DIF_{f_t} = \left(\frac{\dot{\epsilon}}{\dot{\epsilon}_s} \right)^{h\delta} \quad \text{for } \dot{\epsilon} \leq 1 \text{ s}^{-1} \quad (4)$$

$$DIF_{f_t} = \beta \left(\frac{\dot{\epsilon}}{\dot{\epsilon}_s} \right)^{k/3} \quad \text{for } \dot{\epsilon} > 1 \text{ s}^{-1} \quad (5)$$

where DIF_{f_t} is dynamic tensile strength at $\dot{\epsilon}$; $\dot{\epsilon}$ is the strain rate in the range of 10^{-6} – 30 s^{-1} ; $\dot{\epsilon}_s$ is static strain rate, 10^{-6} s^{-1} ; $\log \beta = 6h\delta - 2$; $h \delta = 1/(1 + 8mf'_c/f'_{co})$; f'_c is static compression strength; and f'_{co} is a constant equal to 10 MPa; $m = 0.75$; and $h = 1$, $k = 1$ for H-fiber; $h = 1.3$, $k = 0.8$ for T-fiber.

The values of m , h , k are obtained by applying methods curve fitting accompanied with the trial and error. The parameter m was used to calibrate the compressive strength value f'_c of material to mf'_c , leading to adjust the exponent $h\delta$ in the Eq. (3) and the coefficient β in Eq. (4), and thereby the whole curve was shipped to new position. Thus, m is a parameter representing the difference of strength between concrete and HPFRCC. Since the new position of the curve was geared toward is the black dots of H-fiber (Fig. 16), thus the parameters h and k which are representing the effect of fiber type were assigned 1 in H-case and the other values for T-case with the purpose of rotating the lines a little bit.

The proposed formulation is shown in Fig. 18 for 56 MPa, Ma, and 81 MPa, Mb, and almost matching with the experimental data.

5. Summary and conclusions

This work provides testing results that help to understand the fundamental of the strain rate effects on direct tensile behavior of HPFRCCs. Direct tensile response of HPFRCCs using two types of fiber, hooked and twisted, two types of fiber content, 1% and 1.5% and two types of matrix strength, 56 MPa and 81 MPa, under static and under high strain rate ranging from 10 to 30 s^{-1} was investigated. The following conclusions can be drawn:

- For all the mixes, HPFRCCs maintain strain hardening behavior even at high strain rate condition.

- The T-fibers produce a higher impact resistance, including post cracking strength, strain capacity and peak toughness than H-fibers.
- In improving the impact resistance of HPFRCCs, the strength of matrix plays more important role than the fiber content.
- The rate-sensitivity of HPFRCCs was different according to the types of fiber. In general, the T-fiber produces higher rate-sensitivity of strain capacity. The rate sensitivity of post cracking strength is not clear.
- The rate-sensitivity of HPFRCCs, for all parameters, decreases when the fiber volume content increases from 1% to 1.5%.
- The more increasing of matrix strength, the more rate-sensitivity of strain capacity and peak toughness. The rate sensitivity of post cracking strength is not clear.
- Finally, an equation integrating the effects of fiber type and matrix strength, based on modification of Malvar and Ross' formulation, was introduced to predict the DIF of post cracking strength for HPFRCCs under strain rates ranging from 10^{-6} to 30 s^{-1} .

Acknowledgments

The research described herein was sponsored by Basic Science Research Program through the National Research Foundation of Korea (NRF) funded by the Ministry of Education, Science and Technology (2010-0003161) and by the Human Resources Development of the Korea Institute of Energy Technology Evaluation and Planning (KETEP) grant funded by the Korea government Ministry of Knowledge Economy (No. 20104010100520). The authors are grateful to the sponsors for the financial support. The opinions expressed in this paper are those of the authors and do not necessarily reflect the views of the sponsors.

References

- [1] Naaman AE. Tensile strain-hardening FRC composites: historical evolution since the 1960. In: *Advances in construction materials 2007*, Part II; 2007. p. 181–202.
- [2] Banthia N. Impact resistance of HPFRCC. In: *International RILEM workshop on high performance fiber reinforced composites (HPFRCC) in structural applications*, Honolulu, Hawai'i, USA; 2005. p. 479–88.
- [3] Bindiganavile V, Banthia N, Aarup B. Impact response of ultra-high-strength fiber-reinforced cement composite. *ACI Mater J* 2002;99(6):543–8.
- [4] Yang E, Li VC. Rate dependence in engineered cementitious composites. In: *International RILEM workshop on high performance fiber reinforced composites (HPFRCC) in structural applications*, May 2005, Honolulu, Hawai'i, USA; 2005. p. 83–92.
- [5] Douglas K, Billington SL. Rate dependence in high-performance fiber-reinforced cement-based composites for seismic applications. In: *Proceedings of the 5th international conference on construction materials*, ConMat05, Vancouver, BC, Canada; 2005.
- [6] Maalej M, Quek ST, Zhang J. Behavior of hybrid-fiber engineered cementitious composites subjected to dynamic tensile loading and projectile impact. *J Mater Civ Eng* 2005;17(2):143–52.
- [7] Kim DJ, El-Tawil S, Naaman AE. Rate-dependent tensile behavior of high performance fiber reinforced cementitious composites. *Mater Struct* 2009;42(3):399–414.
- [8] Kim DJ, El-Tawil S, Naaman AE. High performance fiber reinforced cement composites with innovative slip hardening twisted steel fibers. *Int J Concr Struct Mater* 2009;3(2):119–26.
- [9] Cadoni E, Meda A, Plizzari GA. Tensile behaviour of FRC under high strain-rate. *Mater Struct* 2009;42:1283–94.
- [10] Caverzan A, Cadoni E, Prisco M. Tensile behaviour of high performance fibre-reinforced cementitious composites at high strain rates. *Int J Impact Eng* 2012;45:28–38.
- [11] Mechtcherine V, Silva FA, Butler M, Zhu D, Mobasher B, Gao S, et al. Behaviour of strain-hardening cement-based composites under high strain rates. *J Adv Concr Technol* 2011;9(1):51–62.
- [12] Zhu D, Mobasher B, Rajan SD. Non-contacting strain measurement for cement-based composites in dynamic tensile testing. *Cem Concr Compos* 2012;34(2):147–55.
- [13] Tran TK, Kim DJ. Strain energy frame impact machine (SEFIM). *J Adv Concr Technol* 2012;10(3):126–36.
- [14] Tran TK, Kim DJ. Investigating direct tensile behavior of high performance fiber reinforced cementitious composites at high strain rates. *Cem Concr Res* 2013;50:62–73.
- [15] Naaman AE, Shah SP. Pull-out mechanism in steel fibre reinforced concrete. *J Struct Div – ASCE* 1976;102(ST8):1537–48.
- [16] Zielinski AJ, Reinhardt HW. Stress-strain behaviour of concrete and mortar at high rates of tensile loading. *Cem Concr Res* 1982;12:309–11.
- [17] Kang SH, Ahn TH, Kim DJ. Effect of grain size on the mechanical properties and crack formation of HPFRCC containing deformed steel fibers. *Cem Concr Res* 2012;42(5):710–20.
- [18] Kim DJ, El-Tawil S, Naaman AE. Loading rate effect on pullout behavior of deformed steel fibers. *ACI Mater J* 2008;105(6):576–84.
- [19] Nicholas T. Tensile testing of materials at high rates of strain. *Exp Mech* 1981;21(5):177–85.
- [20] Bischoff PH, Perry SH. Compressive behaviour of concrete at high strain rates. *Mater Struct* 1991;24:425–50.
- [21] Lu YB, Li QM. About the dynamic uniaxial tensile strength of concrete-like materials. *Int J Impact Eng* 2011;38(4):171–80.
- [22] Comité Euro-International du Béton. CEB-FIP Model Code 1990. Redwood Books, Trobridge, Wiltshire, UK; 1993.
- [23] Malvar LJ, Ross CA. Review of strain rate effects for concrete in tension. *ACI Mater J* 1998;95(6):735–9.